PHOTOGRAMMETRY MEASUREMENTS OF INITIAL IMPERFECTIONS FOR THE ULTIMATE STRENGTH ASSESSMENT OF PLATES

(DOI No: 10.3940/rina.ijme.2014.a4.294)

A Cubells, Y Garbatov and **C Guedes Soares,** Centre for Marine Technology and Engineering (CENTEC), Instituto Superior Técnico, Universidade de Lisboa, Portugal.

SUMMARY

The objective of the present study is to develop a new approach to model the initial geometrical imperfections of ship plates by using Photogrammetry. Based on images, Photogrammetry is able to take measurements of the distortions of plates and to catch the dominant surface shape, including the deformations of the edges. Having this data, it is possible to generate faithful models of plate surface based on third order polynomial functions. Finally, the maximum load-carrying capacity of the plates is analysed by performing a nonlinear finite element analysis using a commercial finite element code. Three un-stiffened and four stiffened plates have been modelled and analysed. For each plate, two initial imperfection models have been generated one, based on photogrammetric measurements and the other, based on the trigonometric Fourier functions. Both models are subjected to the same uniaxial compressive load and boundary conditions in order to study the ultimate strength.

1. INTRODUCTION

Ship structures are predominantly made of steel plates and stiffeners forming panels. They have widely been used as primary structural components due to the simplicity of their fabrication and high strength-weight ratio. During the service lifetime, these panels are subjected to axial loads and bending moment stresses making the structure susceptible to failure. Despite being the knowledge about the behaviour of these panels still insufficient, it is known that one of the major stability losses is due to buckling of the plates. In order to evaluate the capacity of the plates, the ultimate limit state is used.

The analysis of the ultimate strength of ship structures, taking into account all possible failure modes - plate induced overall buckling (PI), stiffened induced overall buckling (SI), stiffener tripping (ST) and plate buckling (PB) - is not trivial because of the interaction of various factors such as geometry and material properties: loading, boundary conditions, residual stresses and post-weld out-of-plane initial imperfections. The material, with which ship plates are commonly made, is mild or high tensile steel and they can be square or rectangular shape. The loads might be considered in-plane loading, distributed lateral load due to water pressure or a combination of both. The boundary conditions are related to the design of the structure and depend on the position of the plate inside of the structure. The latter factor, the out-of-plane initial imperfections, is the principal factor to be evaluated in this study while the residual stresses are not approached here.

The initial imperfections are generated by manufacturing processes such as welding, cutting and so forth and their influence is of high relevance. During the years, many researchers such as Carlsen and Czujko [1], Guedes Soares [2], Frankland [3] and Smith [4], have studied how the ultimate strength of a plate is affected by the presence of initial imperfections, proposing design methods and equations to predict the ultimate strength. Von Karman and Sechler [5] proposed an equation relating the ultimate strength and the plate slenderness,

$$\beta = \frac{b}{t}\sqrt{\frac{\sigma_0}{E}} \tag{1}$$

Frankland [3], introduced quadratic terms to the former equation and Gerard modified the equation to characterize plates with plastic behaviour. Faulkner [6], proposed a formula for simply supported plates with elasto-plastic behaviour that became one of the most widely used equations on marine structures. Faulkner also found that the presence of the residual stresses reduces the compressive strength by as much as 20% and that the relationship between the non-dimensional amplitude of the initial distortions and the slenderness ratio may be defined as:

$$\phi_u^{Fa} = \begin{cases} 1, & if\ \beta \leq 1 \\ \frac{2}{\beta} - \frac{1}{\beta^2} & if\ \beta \leq 1 \end{cases} \tag{2}$$

$$\left(\frac{W_{max}}{t}\right)_{Fa} = 0.10\,\beta^2 \tag{3}$$

Most of the research concerning the effect of welding distortions concentrates only on the maximum initial distortion amplitude, however, the evidence indicates that the welding distortion shape also significantly affects the ultimate compressive strength [7].

A new formulation was proposed in order to divide the ultimate strength in various terms in an equation that considers two reduction parameters to the maximum ultimate strength, $(\phi_u R_d R_r)$. The first of these parameters regards the initial deflection and the second one, with the residual stresses due to welding. In the past, researchers proposed formulas to evaluate the values for R_d and R_r such as Carlsen [8], Guedes Soares [9], and Cui and Mansour [10].

Among others, Dowling and Frieze [11] alerted that the first buckling mode was not necessary the worst scenario, being necessary to focus to the problem beyond the maximum initial deflection. Antoniou [12] presented a study with 2000 measurements of plates were taken based on the principal mode of deflection. As a result, he proposed a new expression relating the initial deflections as a function of the plate slenderness,

$$\left(\frac{W_{max}}{t}\right)_A = 0.12\,\beta^2 \tag{4}$$

Carlsen and Czujko [1] analysed a typical "hungry horse" shape of initial imperfections in full-scale stiffened panels. This typical shape was found to have the same load-deflection curve with an initial imperfection pattern of three half-sine waves along the length of the plate and one half-sine wave cross across the width of the panel.

Smith, et al. [13] carried out an analysis of initial plate distortions of merchant ships concluding that the dominant distortion, mainly induced by the welding processes followed a sine waves forms. He proposed three levels of initial imperfections and residual stresses in average, slight and severe.

$$\left(\frac{W_{max}}{t}\right)_{Sm} = \begin{cases} 0.025\beta^2 & Slight \\ 0.1\beta^2 & Average \\ 0.3\beta^2 & Severe \end{cases} \tag{5}$$

All the authors considered that the deformations of a plate might be expressed in Fourier expansion series as follows:

$$W_{0,exp} = \sum_{i=1} W_{0,i1} sin\left(\frac{i\pi x}{a}\right) sin\left(\frac{\pi y}{b}\right) \tag{6}$$

where $W_{0,i1}$ is the coefficient of the Fourier series. The number of terms that best represents the initial imperfections, as well as the amplitude of each of them, has been the milestone of the investigations along the years.

The models generated using this trigonometric function present two implicit characteristics, the first is that the edges of the plate is assumed to be equal to 0, and hence, it is assumed that there are no deformations on the edges. The second characteristic is that, since the initial shape of the trigonometric model is symmetric, the response it is expected also to be symmetric in the displacements and stress distribution. These two aspects might bring studies to imprecise results.

Kaminski, et al. [7] stated that the existing simplified methods might be not sufficient to achieve a more advanced buckling and ultimate strength design of ship plating and that more sophisticated solution methods were needed. He outlined the increasing of interest in the evolution of weld induced residual stresses and initial distortions. The prediction of UTS in design stages may bring to more precise calculations of the amount of strength degradation. Having this information, it is possible to identify favourable procedures that maximize the load carrying capacity of structures. In this sense, the present study is aimed to develop a procedure to predict accurately the initial distortions of steel plates and thus, the maximum capacity.

Herein a methodology is developed based on photogrammetric techniques that are able to generate faithful models of the plates to study. This methodology consists in firstly, getting the coordinates of a certain number of points that belong to the surface of the plate on study; secondly, generate a polynomial function that fits to the known points; thirdly, use the functions to generate FEM models that are similar to the real plates and finally, to carry out a non-linear structural analysis using Finite Element Methods (FEM).

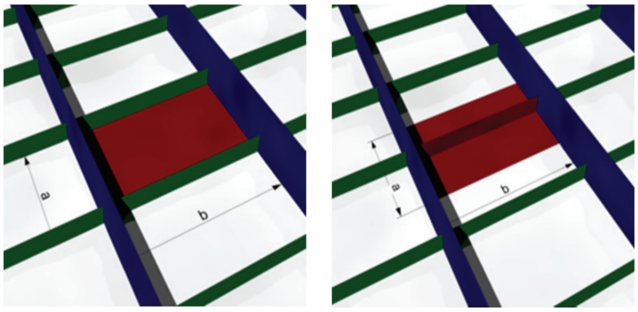

Figure 1. Un-stiffened (left) and stiffened (right) plates

The methodology presented is used to analyse seven real plates. The analysis is done also using Fourier function models and the results are compared. The plates belong to a girder box girder and are specially treated in order to simulate the real characteristics of the plates found in marine structures. The set of specimens is composed by 3 un-stiffened plates (Plate) plus 4 stiffened plates (Stiff) and the location in the whole box girder structure is shown in Figure 1.

Table 1 Specimens

Name	*a, mm*	*b, mm*	t, mm	Wo, mm	a/t
Plate4	175.9	341.6	2.70	2.10	65.1
Plate4_B	180.0	324.7	2.01	2.96	89.5
Plate7	176.1	327.0	2.02	2.82	87.2
Stiff3	189.5	334.2	2.90	2.27	65.3
Stiff4_B	180.0	323.9	2.90	2.05	62.1
Stiff7	175.1	322.3	2.50	2.25	70.0
Stiff 8	189.0	330.2	2.22	2.95	85.2

The aspect ratio of the most of them is approximately equal to 2 and thickness is measured by an ultrasonic gauge. All information is shown in Table 1. The elasticity modulus and the Poisson coefficient are considered to be of E = 206 GPa and $\nu = 0.3$ respectively.

2. PHOTOGRAMETRIC TECHNIQUES

Photogrammetry techniques have been used since 1800 when the idea of representing objects from images started to be attractive. One hundred years later, this technology has been applied in several areas, being predominant in geological and terrestrial representations. More recently, developments have allowed the application of the technology for close-range measurements (i.e. when the size of the object to be measured and the camera-to-object distance is both less than 100 m). Nowadays Photogrammetry is used for measurements of medical, archaeological, architectural and industrial elements, among others.

In the following lines some of the works in which the close-range technology is successfully used are outlined, showing its potential in measuring processes. Koelman [14] presented an industrial application of CAD that concerned the measurements and re-engineering of the shape of a complete ship hull and ship parts. In his study, he considered separately the 3D model measurements and the topological proprieties. Furthermore, in his work he went through a comparison between laser and photogrammetric techniques concluding that the latter is more appropriate for ship hull inverse engineering measurements.

Ljubenkov, et al. [15] used photogrammetry methods in which measurements of the structure deflection in the machinery space and displacements of the main engine are taken before and after the launching. For that experiment there were taken 600 photos to capture 202 measuring points. After the launching, they succeed obtaining structure deflections up to 3 mm at the narrowest parts of the hull with an accuracy of 0.2 mm.
The results of a digital photogrammetric survey, performed on the 81-foot Italian Navy motor yacht “Argo”, were presented by Menna, et al. [16]. 540 circular coded targets were uniformly positioned on the hull surface, and approximately 75 circular code targets were positioned on both the screw propellers. A 12 Mega pixels DSLR camera was used for the image acquisition. About 400 pictures of the boat surface and 60 images per screw propeller were taken with both parallel and convergent camera axes.

A photogrammetric approach for measuring weld-induced initial distortions in plated structures was presented by Chen, et al. [17], [18] and [19], allowing for automatic transfer of the information to finite element models.. Compared with initial imperfection classifications, a new equation to predict the initial imperfections of very-thin-walled structures has been developed.

In the field of civil engineering, Jiang, et al. [20] presented a literature review of close-range photogrammetry applications in bridge deflection measurements. A list of experiences carried out from 1985 to 2003 was presented stating that most of them reached an order of accuracy of about 1 mm. One of the experiences listed was presented by Whiteman, et al. [21] in which two video-camera system were used to measure vertical deflections during destructive tests. Despite of the camera resolution not being as high as a photographic CCD, a precision of 0.25mm was reached, demonstrating the feasibility of obtaining measurements even with low-resolution video camera.

Dias-da-Costa, et al. [22] presented a procedure based on photogrammetry and image post-processing to measure surface displacements in laboratorial test. The aim of that study was to overcome the drawbacks of the traditional methods of measurements. Among those drawbacks were the limitations in hardware positioning, the costs of the equipment and human resources; and time-consuming data processing, as it happens with Displacement-Transducers (LVDT). Therein, it was compared the results obtained by Photogrammetry methods with the measurements coming from LVDT elements. The results showed a high correlation between the values obtained from both systems. The coefficient of determination equals to 0.9994. Similarly, Bambach [23] used a photogrammetric procedure to accurately capture the full surface transverse buckling deformations of the flanges and webs. In his work, he investigated edge-stiffened flanges structures numerically modelled and validated against the experimental results captured by photogrammetric procedures.

Luhmann [24] presented a study summarizing recent developments and applications of digital photogrammetry in industrial measurements. Therein it refers to new concepts for close-range Photogrammetry applications owing to the availability of video and digital cameras in combination with direct access to the digital image data generated. On one hand, off-line system scans are regarded as fully accepted 3D measurement tools that applied in a large variety of industrial application areas, yielding a typical measurement precision on the object in a range of 1:100,000 to 1:200,000 that is 0.1 mm for an object of 10 m size. On the other hand, on-line Photogrammetry systems have the capability of providing measurements in a real time, however, they are less accurate, approximately from 1:4,000 to 1:10,000.

However, it can be stressed that after more than one hundred and fifty years of development, close-range Photogrammetry has been progressed sufficiently in terms of accuracy and practicability. Many experiences have been proven the potentialities of this technique in several fields and the current and quick progress of the cameras and computer processors, make this technology even more eligible modelling structures ensuring high accuracy results.

3. PHOTOGRAMETRIC MODELLING

Photogrammetry is an approach that can determine the size and the shape of objects through analysing images previously recorded by a photographic or video camera. Photogrammetry is divided in two differentiate techniques, analytical and digital. While the principal objective of the present work is to develop a model for the initial imperfection of plates, which is based on analytical Photogrammetry, there are some interesting advantages when using digital Photogrammetry, for example, in corrosion assessment.

The position of an object in space can be defined by a three-dimensional Cartesian coordinate system: the origin, the scale and the orientation of which can be arbitrarily defined. When having more than one photo, it is necessary to convert between coordinates in systems, what it is known as co-ordinate transformation. It can be divided into three parts: scale change, translation and rotation. Change the scale along the three axis depends on the factor λ and may be represented by the vector equation $x = \lambda X$, where $X = [X\ , Y, Z]^t$ is the position vector of a point in the primary coordinate system and $x = [x\ y\ z]^t$ is the position vector of the point in the scaled coordinate system. As for the translation of axes, they may be represented by the following vector equation: $x = X - X_0$, where X is the position vector of a point, in the primary coordinate system, $X_0 = [X_0, Y_0, Z_0]^t$ is the position vector of the origin of the secondary coordinate system, relative to the primary coordinate system and $x = [x\ , y\ , z]^t$ is the position vector of the point in the secondary coordinate system. The rotational process may be expressed as a result of the three independent sequential transformations, correspondent to each axis. For a given point, called A, in a coordinate system (x, y, z), if a rotation ω, φ and k is made clockwise about all axes, the position vector of A in the rotated system $(x_{w\varphi k}, y_{w\varphi k}, z_{w\varphi k})$ system will be $[x_{w\varphi k}, y_{w\varphi k}, z_{w\varphi k}]^t = R_w R_\varphi R_k\ [x, y, z]^t$.

The basic concept for building a functional model in a close range Photogrammetry is the central perspective projection. Being a point called a, three-dimensional positioned point in the space, and its projection onto the projection plane, it is defined as a straight line passing through AO, where O is the perspective centre. At the same time, it defines the straight line POP as an orthogonal one to the projection plane and the distance OP as the principal distance denoted as C (see Figure 2).

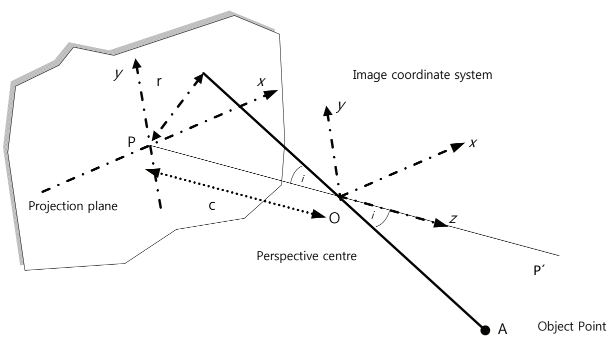

Figure 2. Central perspective projection

In order to derive the functional relationships between the position of the object A and its projection on the projection plane, two co-ordinate systems may be introduced. The primary system $(X\ , Y, Z)$ is arbitrarily located in the object space. In this system, the coordinates of the perspective centre of the secondary system are (X_0, Y_0, Z_0), and the coordinates of the point A are (X_A, Y_A, Z_A). The secondary system (x, y, z) has its origin in O, where the perspective centre is. The z-axis coincides to the orthogonal lines POP, and the x-axis and y-axis are parallel to the ones from the projection plane. Once both coordinate systems are defined, it is possible to write the vectors relative to the primary coordinate system: $X_A = X_0 + S$ where S is the position vector of A relative to O. It is collinear with x_a, but opposite sign:

$$X_A = X_0 - \mu R^t x_a \tag{7}$$

in matrix notation:

$$\begin{bmatrix} X_A \\ Y_A \\ Z_A \end{bmatrix} = \begin{bmatrix} X_0 \\ Y_0 \\ Z_0 \end{bmatrix} - \mu \begin{bmatrix} \gamma_{11} & \gamma_{12} & \gamma_{13} \\ \gamma_{21} & \gamma_{22} & \gamma_{23} \\ \gamma_{31} & \gamma_{32} & \gamma_{33} \end{bmatrix} \begin{bmatrix} x_a \\ y_a \\ -c \end{bmatrix} \tag{8}$$

where μ is a scalar quantity, greater that zero and γ_{ij} are elements of the rotation matrix R.

If now it is considered the same relationship, but this time expressing the primary coordinate system to the secondary one, it is obtained the reverse transformation:

$$x_a = \mu^{-1} R (X_0 - X_A) \tag{9}$$

in matrix notation

$$\begin{bmatrix} x_a \\ y_a \\ -c \end{bmatrix} = \mu^{-1} \begin{bmatrix} \gamma_{11} & \gamma_{12} & \gamma_{13} \\ \gamma_{21} & \gamma_{22} & \gamma_{23} \\ \gamma_{31} & \gamma_{32} & \gamma_{33} \end{bmatrix} \begin{bmatrix} X_0 - X_A \\ Y_0 - Y_A \\ Z_0 - Z_A \end{bmatrix} \tag{10}$$

where the third equation can be explicitly written by μ^{-1} resulting in the following equations:

$$x_a = \frac{-c\ [\gamma_{11}(X_0 - X_A) + \gamma_{12}(Y_0 - Y_A) + \gamma_{13}(Z_0 - Z_A)]}{[\gamma_{31}(X_0 - X_A) + \gamma_{32}(Y_0 - Y_A) + \gamma_{33}(Z_0 - Z_A)]} \tag{11}$$

$$y_a = \frac{-c\ [\gamma_{21}(X_0 - X_A) + \gamma_{22}(Y_0 - Y_A) + \gamma_{23}(Z_0 - Z_A)]}{[\gamma_{31}(X_0 - X_A) + \gamma_{32}(Y_0 - Y_A) + \gamma_{33}(Z_0 - Z_A)]} \tag{12}$$

In the digital Photogrammetry (DP), the photos are taken in a paired stereo configuration and the object's surfaces appearing in them should be of certain characteristics, being the most important its texture and reflective surfaces induce inexact results. Due to its aim, DP can be thought of as camera-based 3D 'Laser-Scanner'. In fact, both systems generate DSM and each one shows some lights and drawbacks depending on the projects to be studied. A deeper comparisons of both systems may be found in [25].

Dense Surface Modelling is based on an algorithm that searches for image patches that 'look' alike from an existing oriented project composed of stereographic photographs. When a good match is found between two photographs, the orientation and camera data allows the program to compute the correct 3D location of the surface point corresponding to the image patch.

4. SURFACE FITTING

The measurements taken from the photogrammetric techniques are used to generate mathematical functions. These functions may be utilized to generate the models of the plates. The reason of using mathematical functions instead of directly using the mesh obtained from photogrammetric techniques relies on the fact that the important information to be considered into the structural analysis is rather the trend of the shape than the plate particularities. It means that the data is filtered and smoothed. Moreover, the straight exchange of mesh data between software often causes erroneous results due to incompatibilities between software. The method used to generate such mathematical functions is based on third polynomial functions.

The initial problem can be defined as follows: given N data points (x_i, y_i) and N numbers $f_i, i = 1,2, \dots, N$, find a function $f(x, y)$ from some class and defined on a plane containing the data points for which $f(x_i, y_i) = f_i$ for $i = 1,2, \dots, N$. The class is defined as the polynomial function of the same order in both x and y and the first four ones are as follows, see Table 2.

Table 2 Polynomial Classes

Class	Basis Function
$\mathcal{P}_0$	1
$\mathcal{P}_1$	1 x y
$\mathcal{P}_2$	1 x y x^2 xy y^2
$\mathcal{P}_3$	1 x y x^2 xy y^2 x^3 x^2y xy^2 y^3

As a result of any fitting, there is a difference between the original coordinates of a point and the coordinates obtained from the calculated function [26]. This difference is defined as $p(x_i, y_i) - f_i$. The objective is then to adjust p by choosing the coefficients $a_0, a_1, a_2, \dots, a_n$ so as to minimize,

$$E(p) = \sum_{i=0}^{N} (p(x_i, y_i) - f_i)^2 \tag{13}$$

$E(p)$ is a function of $a_0, a_1, a_2, \dots, a_n$ and will have a minimum only when $\frac{\partial E}{\partial a_i} = 0$ for $i = 1,2, \dots, 6$. These conditions yield to six linear equations of the unknowns $a_0, a_1, a_2, \dots, a_6$. As for the case of a higher function's class, more coefficients are involved, as it is the case of the cubic functions:

$$\begin{aligned} p(x, y) = a_1 + a_2 x + a_3 y + a_4 x^2 + a_5 xy \\ + a_6 y^2 + a_7 x^3 \\ + a_8 x^2 y + a_9 x y^2 + a_{10} y^3 \end{aligned} \tag{14}$$

Since the number of points composing a project of surface modelling might be of well over 100, it is necessary to call on computer tools. To proceed in finding the coefficients that minimize the difference $p(x_i, y_i) - f_i$, it is used Matlab.

The polynomial degree to be used depends on the complexity of the plate shape to be modelled. If the shape is totally flat, a fitting of first order in both x and y axis would be enough. However, if the plates were fully wavy, it would be necessary to use a higher order. The higher degree allows a more complex shape, nevertheless, the use of higher polynomial degree will involve an increase of the number of coefficients, and hence, the computational efforts. Furthermore, higher degrees functions generate more wavy surfaces, and that could generate erroneous shapes, especially on the borders and corners.

Table 3 R-square of the Polynomial and Fourier functions

X-Deg	Y-Deg	Pl.4B	Pl4L	Pl. 7	St. 3	St.4B	St.7	St. 8
1	1	0.22	0.08	0.09	0.55	0.19	0.06	0.61
2	2	0.81	0.97	0.92	0.81	0.76	0.56	0.71
3	3	**0.95**	**0.98**	**0.98**	**0.97**	**0.96**	**0.68**	**0.81**
4	4	0.97	0.99	0.98	0.98	0.97	0.83	0.85
Fourier model		0.54	0.67	0.73	0.15	0.49	0.04	0.04

Since the dimensions of the specimens studied here have an aspect ratio of approximately 2, not more than two half waves in the longitudinal axis are expected to observe, therefore, at least third polynomial degree is necessary. In order to find the most appropriate function degree, series of fittings from the first to fourth degree (in both axes) has been performed.

Table 3 shows the resultant *R*-square of each case. The trend is drawn by a surface of the second order. It can be observed that the *R*-square increases while the degree in each axis increases. Despite the surface appearing to decrease, when the degree reaches the third order, the R-square obtained is of the same magnitude, meaning that for plates of a/b=2, the third order polynomials are enough to faithfully model their shapes. Table 3 shows that only in one case, a considerable improvement of the adjusted *R*-square is observed, corresponding to stiffened plate No 7. It has been found that while the un-stiffened plates are better adjusted with only one-half wave, the stiffened plates demonstrate higher irregular shapes.

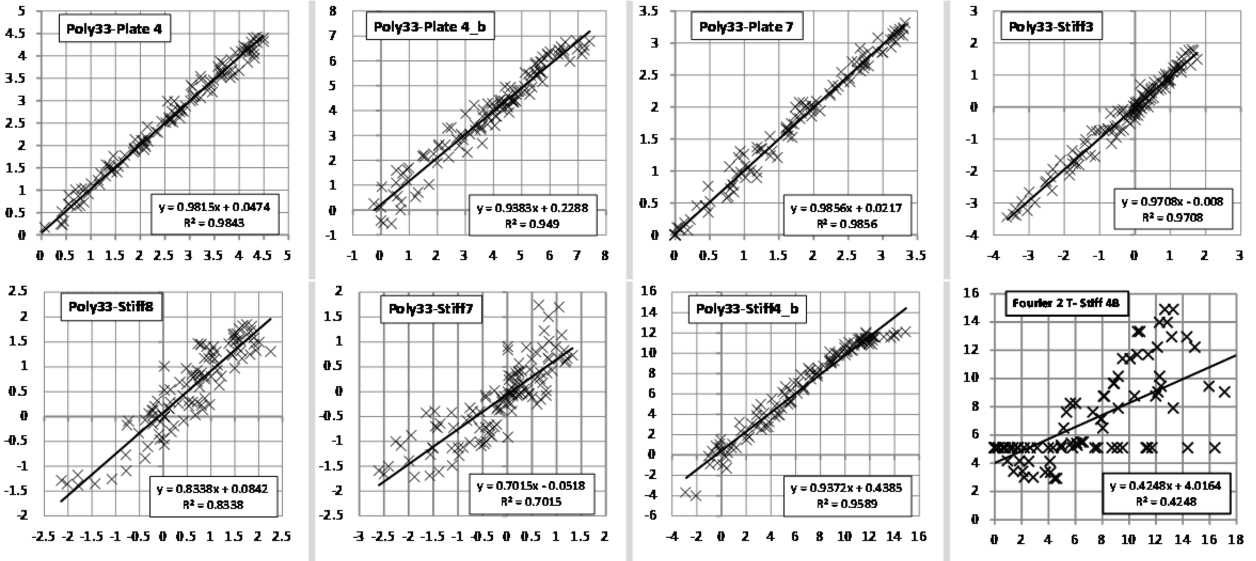

Figure 3 Correlations of the third degree polynomial and Fourier (2 terms) fittings

The correlations (observed-predicted) of the third order polynomials for all the plates are plotted in the Figure 3. Some plates are better represented than others, and that is caused by the distortions from the dominant shape that is found in some case, for example, the stiffened plate No 7. The lower correlations correspond to those cases where the amplitude of the initial deformations is small. Contrarily, if the initial deflections are more evident, the correlation improves. In the same sense, if the plate is extremely deformed, the third order polynomial faces some difficulties to represent the upper values, as it may be seen in the case of the Stiffened 4B plot, where a trend is visible in the upper values.

Furthermore, a comparison with the trigonometric models is carried out. The amplitude of the Fourier terms is calculated using the Custom Function tool from Matlab that finds the coefficients that minimizes the residuals.

The last row of Table 3 shows the *R*-square obtained from the fittings carried out using the Fourier series of 3 terms for the longitudinal direction. In addition, the correlation of a Fourier model of two terms has been performed for the case Stiffened plate 4B and is represented in the last plot in Figure 3.

Despite the fact the accuracy of the photogrammetric measurements may be calculated mathematically, some tests are carried out to prove the correlation between the results and the actual measurements. To do so, three tests are performed; the first one consists in making a plaster cast of a plate. Using a plaster cast permits to take measurements of the out-of-plane distortions by drilling the cast. In the second test, measurements of a very deformed plate (Stiffened 4B) are taken from a quasi-perfect plate. The plate to study and the quasi-perfect plate are faced one to each other, and since the quasi-perfect plate is drilled, a calliper may be used to take measurements. The third test consists in dispose of 161 points over a surface that is as much flat as possible. The goal is to check out if Photogrammetry is able to catch such flatness.

Table 4 GOF of the tests

	SSE	Mean	SSR	SST	ST.DV	R^2
Test 1a	121.0	6.72	1845	1966	1.17	0.938
Test 1b	97.1	6.72	1694	1791	1.05	0.946
Test 1c	76.7	5.27	2233	2309	0.94	0.964
Test 1d	89.6	5.24	2242	2332	1.01	0.958
Test 2a	0.3098	0.02	53	53	0.05	0.995
Test 2b	0.1518	0.00	61	61	0.04	0.998
Test 3	9.9	84.44	184061	184071	0.25	0.9999

The results of the test draw high correlated values, *R*-squares from 0.938 up to 0.998 (Table 4). However, it should be considered that some deviations may be attributed to the inaccuracies of taking measurements or the difficulty of generating absolutely perfect flat planes.

5. STUDY CASE

In order to carry out the strength assessment of plates, a methodology that integrates all the steps involved in the analysis is developed. The procedure is represented in Figure 4, which is mainly composed by three stages that are coincident with three techniques: Photogrammetric modelling, Surface Fitting, and Finite Element Analysis.

The methodology is designed in a way that all the data involved in the procedure are properly suited and able to be used in the following stages.

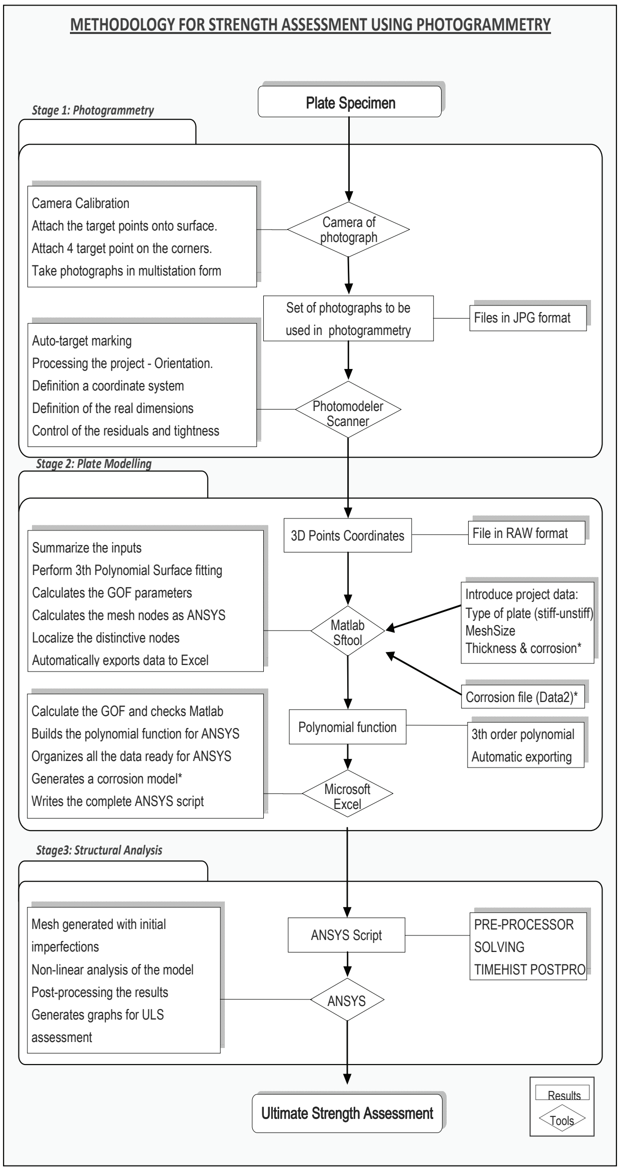

Figure 4 Strength assessment methodology

5.1 STAGE 1: PHOTOGRAMMETRY

To solve the photogrammetric equations, a commercial code called Photo-modeller [27] has been used. This program helps in extracting the measurements and 3D models from photographs, by using a camera as an input device. The model can be created automatically by using auto referencing marking codes with the so-called *Automatic Target Marking*. This procedure is used to model the plates since it is more reliable and faster than manual picking.

The camera used in this study is a Sony Alpha 100, which is able to shoot photos up to 10 Megapixels. Before to start, it is necessary to calibrate the camera and the lens under the conditions that are going to be used as it is the focal length. The quality of the results obtained in the project depends very much on the quality of the calibration.

The objective is to model the deflections of the plates, and the way to do it is by attaching reference points onto the surface of the plates, following the shape. These reference points are known as coded target points and they are physical codified points whose the program is able to find inside of a photograph. In order to ensure that the target points follow the shape of the plates with more fidelity, the targets are disposed in magnetic strips.

From the solution of the collinearity equations, the program is able to measure the accuracy of the project by measuring the distances between the expected point coordinates and the ones observed in the photographs, that is, the residuals. As a reference, a maximum of 1 pixel residual is considered for an acceptable measurement.

Table 5 shows the qualitative values of the projects carried out with Photo - modeller. In 5 cases, 8 photos are taken per plate and in two cases, only 4 photographs were used attaining the same order of accuracy. Figure 6 shows an example of two points of clouds representing the plates.is shown.

Table 5 Qualitative values of the projects

Name	Nº Ph.	Coverag e	Overall RMS	Max RMS	Min RMS
			mm		
Stiff 8	8	89%	0.022	0.033	0.022
Stiff3	8	89%	0.059	0.081	0.057
Plate7	8	88%	0.027	0.029	0.026
Plate4	8	89%	0.019	0.021	0.019
Stiff7	8	89%	0.018	0.021	0.017
Plate4_ B	4	89%	0.034	0.092	0.029
Stiff4_B	4	89%	0.015	0.025	0.014

The result of the photogrammetric stage is the coordinates of a set of points that represents the surface of the plate. These coordinates are saved in a JPG file that is used to generate the polynomial functions that will be utilized to generate the model.

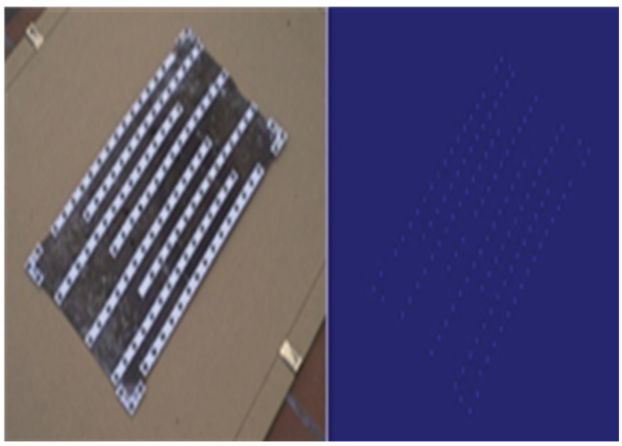

Figure 5 Plate modelling with target points.

5.2 STAGE 2: PLATE MODELLING

A procedure to generate a script for the finite element software ANSYS [28] is presented here. This takes into account the data of the plate and other parameters that are necessary such as the thickness. ANSYS scripts may be created automatically by using two programs, Matlab and MS Excel. Figure 6 shows all data necessary to proceed and the sequence of its use through all the programs.

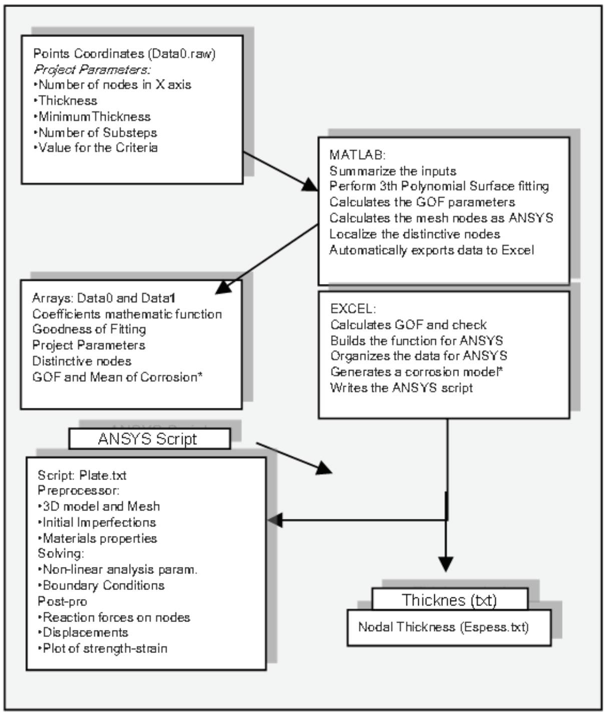

Figure 6. Data collection methodology

A macro in Matlab is written to automatically carry out the third polynomial surface fitting and to calculate the polynomial coefficients based on the points' coordinate computed by Photomodeller. The macro also calculates the mesh size about the number of nodes in X-axis and generates an array with nodes that will be further created by the ANSYS pre - processor and their coordinates.

All the data generated by Matlab is stored automatically to an Excel's file. This file is previously designed in such a way is able to read the data stored by Matlab and generate a script file to be run with ANSYS program.

5.3 FINITE ELEMENT ANALYSIS

The plates are modelled by nonlinear shell elements SHELL181 of four nodes and each node has 6 degrees of freedom. This type of element permits to set up non-linear and multi-linear material properties. The nonlinear material properties are defined as MISO, that is, multi-linear isotropic with hardening. The convergence of the mesh size has been studied and it has been proven that the model converges monotonically. From this check it can be concluded that no significant improvements are obtained for meshes finer than 1,000 nodes.

The analysis has been carried out for both approaches, one based on the Fourier Functions approach and the second one is based on the photogrammetric measurements. In the first case a maximum amplitude of $w_0 = 0.12\,\beta^2$ has been considered as proposed by Antoniou [12]. Initially, the non-stiffened plates are studied: Plate 4, Plate 4B (Figure 7) and Plate 7 (Figure 8), where σ/σ_y (stress/Yield stress) is presented as a function of $\varepsilon/\varepsilon_y$ (strain/Yield strain). For this study the plates are considered not to be affected by the corrosion. As the initial imperfections increases a decrease of the load carrying capacity of the plates and the ultimate strength is seen in the half of the Yield stress approximately. As it can be seen, in the two cases representing the UTS reached in the models where the initial imperfection is generated by using the Fourier functions are slightly higher than the ultimate strength capacity attained in the models based on the photogrammetric measurements.

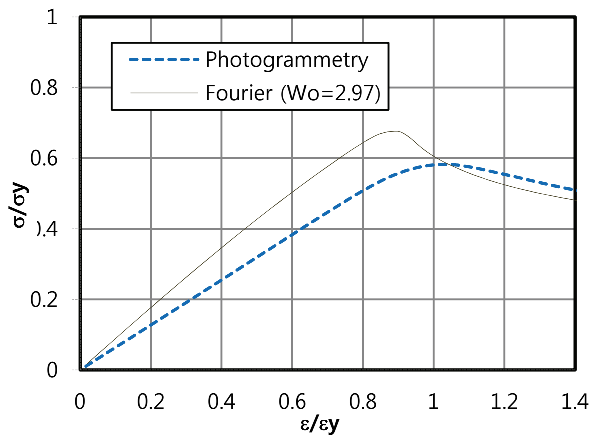

Figure 7 Strength-strain ratio, unstiffened plate 4B

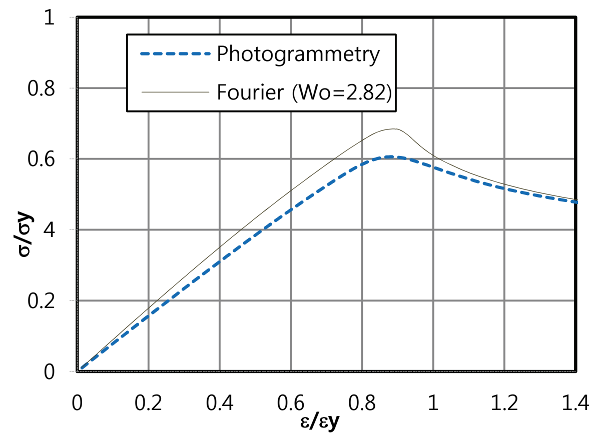

Figure 8 Strength-strain ratio, unstiffened plate 7

In order to find out the reason for that, Plate 4B is studied in more detail. Figure 9-left plots the $z - axis$ displacement and Figure 9-right, the Von Misses stresses for the case modelled using the Photogrammetry measurement is Figure 9 (down) and Figure 9 (up) for the Fourier functions. It is clear that symmetry in both axes is found from the beginning to the end of the load application, resulting in the ultimate strength for the Fourier function modelling of the initial imperfection. In contrary to that, the Photogrammetry modelling of the initial imperfection induces asymmetry in displacement and stresses, what brings to a lower overall ultimate strength of the model.

Similar analysis has been made for the stiffened plates. Because of the presence of the stiffener attached to the plate and due to the fact that the boundary conditions are different, the results obtained are different. It seems that stiffened plate 4, 7 and 8 are performing in a similar manner. This is because of the fact that the initial deformations of the specimen 4B conduce an overall plate buckling.

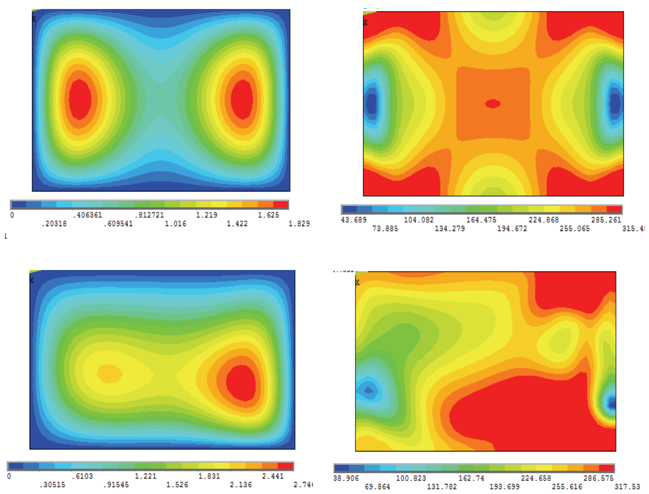

Figure 9. Plate 4B displacement (left) and von Misses stresses (right) for Fourier (up) and Photogrammetry (down) initial imperfection models

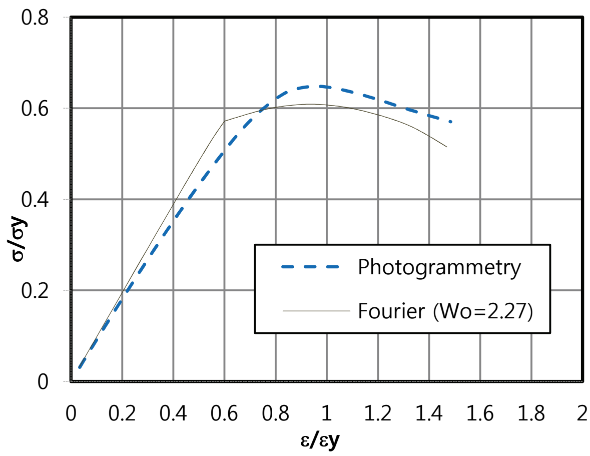

Figure 10. Strength-strain ratio, stiffened plate 4

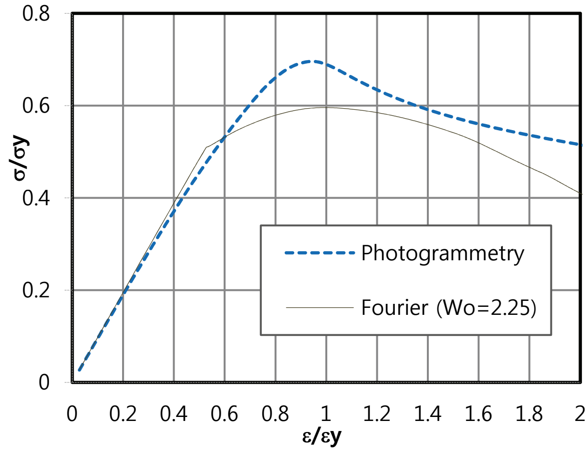

Figure 11. Strength-strain ratio, stiffened plate 7

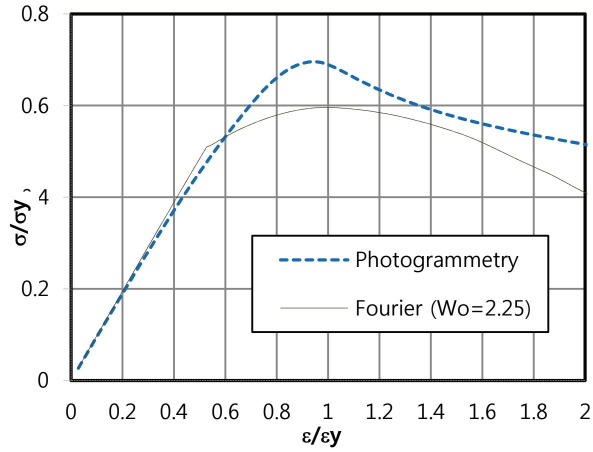

Figure 12. Strength-strain ratio, stiffened plate 8

It has been seen that the asymmetries cause a strength reduction in the case of the un-stiffened plates, however, in stiffened ones, the asymmetries may cause a rise of the ultimate strength, compared to the ones obtained with the Fourier model on the initial imperfection.

Checking the plots of displacement it may be seen that the plates are influenced not only by the slenderness but also by the shape of the initial imperfection. Within the pre-buckling part, the initial imperfections are amplified once the load is applied and as the buckling capacity is approached, the plate gradually changes the shape in order to adapt its lowest energy shape. In the case of the Fourier models, the initial dominant shape is one-half sine wave since this corresponds the lowest energy shape. The transition from the first shape to the other is done in a short piece of time and consequently the strength-strain curve presents a sharp slope change.

On the other hand, the models analysed using photogrammetric measurements to model the initial imperfection present asymmetries in both axis of the plates. These asymmetries are found to be very influential in the behaviour for two reasons: the first one is related to the shape of the initial imperfection, which for the initial imperfection modelled by the Fourier functions are found to be of two-half sine waves, and in the photogrammetric modelling of the initial imperfection are of different shapes in each case. As an example, Figure 14 to 15 show the displacement shapes of plates 3 and 8 at the ultimate strength capacity.

The plots in Figure 14 to 15 on the left correspond to the plate modelled using the trigonometric Fourier functions and the plots on the right show the model based on the photogrammetric measurements.

As can be seen, the displacements of the Fourier models are symmetric and the lowest energy shape has always been found to correspond to the second mode of deformation (i.e. two-half sine waves). On the other hand, the shape of the photogrammetric models at the ultimate strength point may adopt various forms, being dominated by the initial out-of-plane deformation, and because of that, the strength varies in each case.

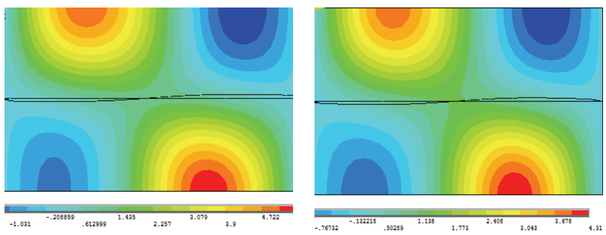

Figure 13. Displacements at the ultimate strength, Stiff 3, Fourier (left) and Photogrammetry (right) models.

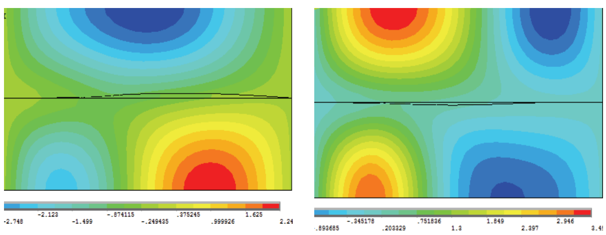

Figure 14. Displacements at the ultimate strength, Stiff 8, Fourier (left) and Photogrammetry (right) models.

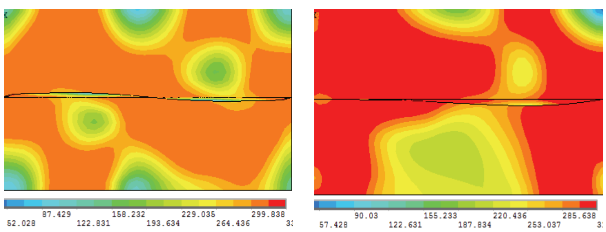

Figure 15. Stress distribution, Stiff 7, Fourier (left) and Photogrammetry (right) model,

The second reason is related to the transition of the shapes during the loading process that plates adopt. Since the distortions of the initial imperfection of the photogrammetric models are more dominant than the one of the Fourier cases, the plates do not go through any transition, and thus, there is no any sudden change of the strength-strain curve slope. The asymmetries observed in the displacements are also noticeable in the von Misses stress plots. Figure 16 represents a stress distribution of the stiffened plate 7 when the ultimate strength is reached.

6. DISCUSSION

The ultimate strength of plates based on different initial imperfection models: modelled using the Fourier functions and photogrammetric functions from the photogrammetric measurements are shown in Table 6. The un-stiffened plates show more optimistic ultimate strength in the models based on the Fourier functions than the ones of the photogrammetric models. In the case of the stiffened plates, more optimistic results are obtained from the photogrammetric models unless the Plate 4B, due to the large initial deformations.

Table 6 Ultimate Strength

Name	σ_u/σ_y (Fourier)	σ_u/σ_y (Photogrammetry)
Plate4	0.78	0.74
Plate4_B	0.68	0.58
Plate7	0.68	0.61
Stiff3	0.61	0.65
Stiff4_B	0.65	0.22
Stiff7	0.60	0.70
Stiff 8	0.50	0.55

The results obtained from the photogrammetric models are more varied and even in one case -stiffened 4B - the results are completely different from the Fourier models. This is explained by the fact that the models based on Photogrammetry consider the geometrical particularities of each plate that might be deformed in a different manner than the others.

When comparing the behaviour of unstiffened plates modelled on Fourier and Photogrammetric basis, the following points may be drawn.

The deformation shapes of the unstiffened plates modelled by the Photogrammetry are similar to those generated by the trigonometric Fourier functions, because the dominant shape of deformation corresponds to the first mode of deformation, which is the mode that the Fourier function can model best. However, two singularities are still remarkable: the small asymmetries that are not considered in Fourier models and the out-of-plane borders. These singularities and the fact that the initial amplitude is different than the one obtained for Fourier functions, bring the results to be different.

The difference in ultimate strength between the two modelling types is approximately of 10%. The lower ultimate strength obtained from the photogrammetric models might be explained by the asymmetries found in those models.

The more differentiate strength-strain curve corresponds to plate 4B, that it is found to be with a more asymmetrical shape of the initial imperfection. The differences are found not only in the ultimate strength, but also in the strain that it is reached.

From the comparison between the behaviour of stiffened plates with initial imperfections modelled with the Fourier and Photogrammetric approach, the following points may be drawn.

The strength-strain curves obtained from models based on the Fourier and Photogrammetric approach are slightly different in terms of the shape as well as the ultimate strength capacity.

In the case of the un-stiffened plates, the asymmetry causes an ultimate strength reduction for the photogrammetric models. On the other hand, it seems to provoke a strength improvement in the case of stiffened plates. Such effect can be explained with the initial shape of the imperfection which strengthens the specimen.

7. CONCLUSIONS

Along the years, the initial imperfections of plates have been modelled using the Fourier functions to assess their load carrying capacity. In this study, a new approach based on photogrammetric measurements is proposed. This approach generates models that take into account the real shape of plates instead of relying in statistical approaches.

The approach involves several steps that are identified and organized in such a way that the analysis can be carried out in an easy and reliable manner. The procedure is composed of three stages that are coincident with three techniques: Photogrammetric modelling, Surface Fitting, and Finite Element Analysis. In order to achieve the final goal, an integrated solution that manages the data along the process is established.
Based on this methodology, faithful geometry models of seven plates, three unstiffened and four stiffened ones, originally belonging to a box girder have been generated and used to carry out a FEM analysis. The results of analyses have been compared, demonstrating that the photogrammetric models are able to catch the asymmetries present in the real plate surfaces. It has been found that these asymmetries are very important and influence the maximum capacity of the structures.

8. REFERENCES

1. CARLSEN, C. A. and CZUJKO, J., The Specification of Post-welding Distortion Tolerances for Stiffened Plates in Compression, The Structural Engineer, 56A, (5), pp. 133-141, 1978.
2. GUEDES SOARES, C., Uncertainty Modelling in Plate Buckling, Structural Safety, 5, pp. 17-34, 1988.
3. FRANKLAND, J. M., The Strength of Ship Plating under Edge Compression, U.S Experimental Model Basin Progess Report, 469, 1940.
4. SMITH, C., Compressive Strength of Welded Steel Ship Grillages, Trans RINA, 117, pp. 325–359, 1979.
5. VON KARMAN, T. and SECHLER, E. E., The Strenth of Thin Plates in Compression, Transactions of ASME, 54, pp. 53-57, 1932.
6. FAULKNER, D., A Review of Effective Plating for use in the Analysis of Stiffened Plating in Bending and Compression, Journal of Ship Research, 19, pp. 1-17, 1975.
7. KAMINSKI, M., AMDAHL, J., FASANO, E., FRIEZE, P., GORDO, J. M., GRUNDY, P., HESS, P. E., KAWAMOTO, Y., KUJALA, P., PAIK, J., ROHR, U. and SIMONSEN, B., Committee VI.2 Ultimate Hull Girder Strength, Proceedings of the 14th International Ship and Offshore Structures Congress (ISSC), H. Ohtsubo and Y. Sumi, Nagasaki, Japan, Vol. 1, pp. 321-391, 2000.
8. CARLSEN, C. A., Simplified Collapse Analysis of Stiffened Plates, Norwegian Maritime Research, 5, (1-4), pp. 135-177, 1977.
9. GUEDES SOARES, C., Design Equation for the Compressive Strength of Unstiffened Plate Elements with Initial Imperfections, Journal of Constructional Steel Research, 9, pp. 287-310, 1988.
10. CUI, W. and MANSOUR, A., Effects of Welding distortions and residual stresses on the ultimate strength of long rectangular plates under uniaxial compression., Marine Structures, 11, (6), pp. 251-269, 1988.
11. DOWLING, P. J. and FRIEZE, P. A., Ultimate Load Behavior of Plates in Compression, Steel plated Structures: International symposium, P. J. Dowling, J. E. Harding and P. A. Frize, London, pp. 24-50, 1977.
12. ANTONIOU, A. C., On the Maximum Deflection of Plating in Newly Built Ships, Journal of Ship Research, 24, (1), pp. 31-39, 1980.
13. SMITH, C. S., DAVIDSON, P. C., CHAPMAN, J. C. and DOWLING, J. P., Strength and Stiffness of Ships' Plating under In-plane Compression and Tension, Transactions RINA, 130, pp. 277-296, 1988.
14. KOELMAN, H., Application of a Photogrammetry-based System to Measure and Re-engineer Ship Hulls and Ship Parts: An Industrial Practices-based Report, Computer-Aided Design, 42, (8), pp. 731-743, 2010.

15. LJUBENKOV, B., ZAPLATIC, T. and ZIHA, K., Measurements for Reliability of Ship Production and Operation. In: Advanced Ship Design for Pollution Prevention, C. Guedes Soares and J. Parunov, editors, London: Taylor & Francis Group, pp. 281-288, 2010.
16. MENNA, F., ACKERMANN, S., SCAMARDELLA, A. and TROISI, S., Digital Photogrammetry: A Useful Tool For Shipbuilding Applications, Proceedings of the 13th Congress of International Maritime Association of Mediterranean, IMAM, Istanbul, Turkey, pp. 607-614, 2009.
17. CHEN, B. Q., GARBATOV, Y. and GUEDES SOARES, C., Displacement Measurement of Box Girder Based on Photogrammetry, Proceedings of the 11th International Symposium on Practical Design of Ships and other Floating Structures (PRADS 2010), paper PRADS2010-20083, S. Spaier, S. Estefen and I. Pasqualino, Rio de Janeiro, Brasil, 2010.
18. CHEN, B. Q., GARBATOV, Y. and GUEDES SOARES, C., Automatic Approach for Measuring Deformations in Complex Structures Using Photogrammetry Technique, Proceedings of the XXII Pan American Conference of Naval Engineering, Maritime Transportation & Ports Engineering, Buenos Aires, Argentina, 2011.
19. CHEN, B. Q., GARBATOV, Y. and GUEDES SOARES, C., Measurement of Weld Induced Deformations in Three-dimensional Structures Based on Photogrammetry Technique, Journal of Ship Production and Design, 27, (2), pp. 51-62, 2011.
20. JIANG, R., JÁUREGUI, D. V. and WHITE, K. R., Close-range Photogrammetry Applications in Bridge Measurement: Literature Review, Measurement, 41, (8), pp. 823-834, 2008.
21. WHITEMAN, T., LICHTI, D. D. and CHANDLER, I., Measurements of Deflections in Concrete Beams by Close-range Digital Photogrammetry, Symposium on Geospatial Theory, Processing and Applications Ottawa, 2002.
22. DIAS-DA-COSTA, D., VALENÇA, J. J. and EDUARDO, N. B. S., Laboratorial Test Monitoring Applying Photogrammetric Post-processing Procedures to Surface Displacements, Measurement, 44, (3), pp. 527-538, 2011.
23. BAMBACH, M. R., Photogrammetry Measurements of Buckling Modes and Interactions in Channels with Edge-stiffened Flanges, Thin-walled Structures, 47, (5), pp. 485-504, 2009.
24. LUHMANN, T., Close Range Photogrammetry for Industrial Applications, ISPRS Journal of Photogrammetry and Remote Sensing, 65, (6), pp. 558-569, 2010.
25. ZAPLATIC, T., GOMERCIC, M., LJUBENKOV, B. and BAKIC , A., Dimensions and Shape Control of the Sub-assembled Sections using Digital Photogrammetry, Schiffbauforschung, 47, (1), pp. 68-83, 2008.
26. LANCASTER, P. and SALKAUSKAS, K., Curve and Surface Fitting: Harcourt Brace Jovanovich, 1987.
27. PhotoModeler®, Eos Systems Inc., www.photomodeler.com/index.htm 2009.
28. Ansys, Online Manuals.Release 12, 2009.

